## Dark-Matter-Induced Nucleon Decay Signals in Mesogenesis

Joshua Berger<sup>1,\*</sup> and Gilly Elor<sup>2,†</sup>

<sup>1</sup>Colorado State University, Fort Collins, Colorado 80523, USA

<sup>2</sup>Weinberg Institute, Department of Physics, University of Texas at Austin, Austin, Texas 78712, USA

(Received 1 March 2023; revised 16 November 2023; accepted 24 January 2024; published 20 February 2024)

We introduce and study the first class of signals that can probe the dark matter in mesogenesis, which will be observable at current and upcoming large volume neutrino experiments. The well-motivated mesogenesis scenario for generating the observed matter-antimatter asymmetry necessarily has dark matter charged under the baryon number. Interactions of these particles with nuclei can induce nucleon decay with kinematics differing from spontaneous nucleon decay. We calculate the rate for this process and develop a simulation of the signal that includes important distortions due to nuclear effects. We estimate the sensitivity of DUNE, Super-Kamiokande, Hyper-Kamiokande, and JUNO to this striking signal.

DOI: 10.1103/PhysRevLett.132.081002

Mesogenesis mechanisms [1–4] utilize the *CP* violation of standard model (SM) meson systems to generate the primordial baryon asymmetry and the dark matter (DM) abundance of the Universe. Excitingly, mesogenesis is highly testable [5,6] and experimental searches are underway to probe signals directly linked to the generated baryon asymmetry [6–10] (see overviews in [11–14]). However, a direct probe of the DM in mesogenesis remained elusive, until now. In this Letter, we study DM-induced nucleon decays (INDs) in mesogenesis, which can produce striking signals at current and upcoming neutrino detectors. While the mesogenesis framework is the focus of this Letter, methods developed here can be broadly applied to search for models containing dark baryons, e.g., [15–17].

The novel way in which mesogenesis satisfies the Sakharov conditions [18] is as follows: mesons produced at late (MeV scale) times, having undergone CP-violating processes, decay out of equilibrium into dark baryons. This process generates an equal and opposite baryon asymmetry between the dark and visible sector, e.g., in  $B^0$  mesogenesis [1] the baryon asymmetry is generated from the late time production of  $B^0_{s,d}$  mesons that undergo CP-violating oscillations before quickly decaying into a SM baryon and a dark Dirac fermion  $\psi_{\mathcal{B}}$  carrying SM baryon number -1. To evade washing out the generated baryon asymmetry through, e.g.,  $\psi_{\mathcal{B}} \to pe\bar{\nu}_e$ , the  $\psi_{\mathcal{B}}$ 's must rapidly decay into stable DM states.

Mesogenesis DM consists of a dark Majorana fermion  $\xi$  and a dark complex scalar  $\phi_{\mathcal{B}}$ , which is charged under SM

Published by the American Physical Society under the terms of the Creative Commons Attribution 4.0 International license. Further distribution of this work must maintain attribution to the author(s) and the published article's title, journal citation, and DOI. Funded by SCOAP<sup>3</sup>. baryon number. These two stable particles compose the entirety of DM, i.e., the DM halo will consist of a mixture of  $\xi$  and  $\phi_{\mathcal{B}}$  that can scatter off target nuclei in neutrino detectors to produce monoenergetic mesons and missing energy. This process of IND appears experimentally as nucleon decay but with different kinematics, as such current limits are not constraining.

The cross section for IND, as it arises in mesogenesis, will be within reach of neutrino detectors and can be searched for at the Deep Underground Neutrino Experiment (DUNE) [19], Super-Kamiokande [20], Hyper-Kamiokande [21], and JUNO [22]. Furthermore, given the monoenergetic (up to smearing effects) meson, such signals should be distinct over SM backgrounds, primarily due to atmospheric neutrino processes.

To study the details of the IND process, we developed a Monte Carlo event generation tool within the GENIE [23,24] software suite used to study neutrino scattering events [25]. We can then study the detailed kinematics of the outgoing mesons produced during DM scattering events and compare these with the dominant atmospheric neutrino scattering background. The event generation includes nuclear effects that smear out the spectrum of mesons from one that is nearly monoenergetic in the nonrelativistic DM limit. Furthermore, these events are ready to be used for study in neutrino experiments, where they can be passed through detector-specific simulation software.

In this Letter, we first characterize the IND signal. We present the mesogenesis-specific parameter space that can be targeted by experiments. We then detail the simulation. Next, we apply this simulation to estimate the sensitivity of experiments.

Characterizing the IND signal.—Generating the baryon asymmetry in B mesogenesis [1,3], requires the existence of a TeV scale colored scalar [26], which mediates the

baryon number conserving decay of a B to  $\psi_B$  and a SM baryon through the (GeV scale) effective operator

$$\mathcal{O}_{ab,c} = C_{ab,c} \epsilon_{ijk} \left( u_a^i d_b^j \right) (\psi_{\mathcal{B}} d_c^k), \tag{1}$$

where all fermions are right handed, though our results generalize to left-handed operators.  $C_{u_ad_b,d_c} \equiv y_{u_ad_b}y_{\psi d_c}/M_Y^2$ , where  $M_Y$  is the mediator mass.  $\psi_{\mathcal{B}}$  decays to the DM through  $\mathcal{L}_d \supset y_d \bar{\psi}_{\mathcal{B}} \xi \phi_{\mathcal{B}} + \text{H.c.}$ , which is allowed by a stabilizing  $\mathbb{Z}_2$  symmetry under which  $\psi_{\mathcal{B}}$  is even and the DM particles are odd.  $y_d$  is a free parameter, but a motivated benchmark is  $y_d \lesssim \mathcal{O}(0.1)$ , which results in the correct DM abundance given an example UV embedding [4].

Equation (1) generates the IND signal in mesogenesis: when kinematically allowed, an incoming  $\xi$  or  $\phi_B$  scatters off a proton or neutron by exchanging a  $\psi_B$  and produces an energetic meson. Figure 1 depicts an example process—incoming  $\phi_B$ 's induce proton decay to  $\pi^+$  through  $\mathcal{O}_{ud,d}$ . Similarly, IND to kaons arises through  $\mathcal{O}_{ud,s}$  and  $\mathcal{O}_{us,d}$ . We consider searches for the processes

$$\phi_{\mathcal{B}}N \to \mathcal{M}\xi$$
 if  $m_{\phi_{\mathcal{B}}} + m_N > m_{\mathcal{M}} + m_{\xi}$ , (2a)

$$\xi N \to \mathcal{M} \phi_{\mathcal{B}}^{\star}$$
 if  $m_{\xi} + m_{N} > m_{\mathcal{M}} + m_{\phi_{\mathcal{B}}}$ , (2b)

where  $N = n^0$ ,  $p^+$  and  $\mathcal{M}$  is a SM meson. Recall that  $\xi$  is Majorana, allowing any of the DM states to participate in this process when it is kinematically allowed. For decays induced by incoming  $\phi$ 's, the kinetic energy of the outgoing meson, to  $\mathcal{O}(v_{\rm DM})$ , is given by

$$E_{\phi_B N \to \xi \mathcal{M}}^{\mathcal{M}, \text{kin}} = \frac{m_{\mathcal{M}}^2 - m_{\xi}^2 + (m_N + m_{\phi_B})^2}{2(m_N + m_{\phi_B})} - m_{\mathcal{M}}.$$
 (3)

Swap  $m_{\xi} \leftrightarrow m_{\phi_{\mathcal{B}}}$  to obtain the meson energy from incoming  $\xi$ 's.

If the struck nucleon is at rest, then the outgoing meson is monoenergetic with energy given in Eq. (3). However, the nucleons are moving with a momentum of  $\mathcal{O}(100 \text{ MeV})$  inside nuclei, smearing out of the meson signal (except for the case of scattering off hydrogen in water Cherenkov detectors). We simulate the IND process, carefully accounting for this smearing. Note that the energies of these decays

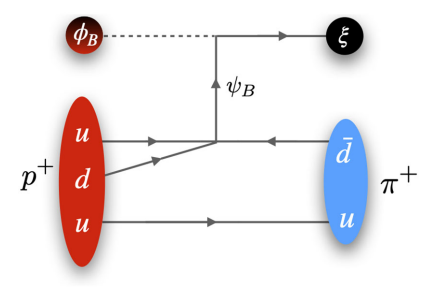


FIG. 1. Induced proton decay to a pion through  $\mathcal{O}_{u,dd}$ .

are shifted compared to spontaneous nucleon decay, with higher energies when  $\phi_B$  scatters and lower energies when  $\xi$  scatters. This alters the phenomenology of the mesogenesis scenario compared with proton decay models such as grand unified theories, the targets of current nucleon decay searches [27–32]. As such, existing limits from nucleon decay searches do not generally constrain the mesogenesis signal [33].

The cross section for IND is obtained from the matrix element

$$\mathcal{A}_{\phi_{B}N \to \xi \mathcal{M}} = \bar{u}_{\xi}(\vec{p}_{\xi}) \frac{y_{d}C_{ab,c}}{p_{\psi_{B}}^{2} - m_{\psi_{B}}^{2}} (\not p_{\psi_{B}} + m_{\psi_{B}}) \times P_{R} \left[ W_{0}^{RR} - i \frac{\not p_{\psi_{B}}}{m_{N}} W_{1}^{RR} \right] u_{N}(\vec{p}_{N}), \quad (4)$$

with  $\bar{u}_{\xi} \to \bar{v}_{\xi}$  for  $\xi N \to \mathcal{M} \phi_{\mathcal{B}}^{\star}$ . Here,  $p_{\psi_B} = p_{\xi} - p_{\phi_B}$  and  $P_R$  is the right-handed fermion projector. The Wilson coefficients are constrained by a combination of LHC searches for the mediator and flavor observables:  $C_{ud,d}^{\max} = 0.07$  and  $C_{ud,s}^{\max}$ ,  $C_{us,d}^{\max} = 0.64$  TeV<sup>-2</sup> [6,15]. Since INDs can lead to  $\mathcal{O}(\text{GeV})$  momentum transfer, we use high  $q^2$  extrapolated lattice results for the form factors  $W_{0,1}^{RR}$  [35,36]. Including the momentum dependence of  $W_{1,2}$  negligibly affects the signal.  $\mathcal{O}_{us,d}$  and  $\mathcal{O}_{ud,s}$  require different form factors, but lead to similar signals.

Mesogenesis parameter space.—In addition to the kinematic constraints on IND, Eq. (2), the allowed parameter space is constrained by mesogenesis-specific considerations, i.e., generating the observed baryon asymmetry and DM abundance.

$$m_{\phi_B} + m_{\xi} < m_{\psi_B} < m_B - m_p \simeq 4.34 \text{ GeV},$$
 (5a)

$$|m_{\phi_B} - m_{\xi}| < m_p + m_e \simeq 938.8 \text{ MeV},$$
 (5b)

$$m_{\psi_{\mathcal{B}}}, m_{\phi_{\mathcal{B}}} > m_p - m_e.$$
 (5c)

$$m_{\phi_{\mathcal{B}}} > m_{\xi}.$$
 (5d)

The regions in  $\{m_{\xi}, m_{\phi_{\mathcal{B}}}\}$  space excluded by these constraints are shaded in Fig. 2, while the white region is allowed. Equation (5a) ensured that  $\psi_{\mathcal{B}}$  is light so that the baryon asymmetry can be generated through the decay  $B \to \mathcal{B}_{\rm SM} + \psi_{\mathcal{B}}$ , while also being heavy enough to decay into the DM  $\xi$  and  $\phi_{\mathcal{B}}$ . Decreasing the value of  $m_{\psi_{\mathcal{B}}}$  corresponds to increasing the excluded green region. For  $m_{\psi_{\mathcal{B}}} \simeq 1.1$  GeV, there is no longer viable parameter space. Equation (5b) is enforced to prevent  $\xi$  and  $\phi_{\mathcal{B}}$  from coalescing into SM baryons, which would wash out the asymmetry. Proton decay through Eq. (1) to dark baryons is kinematically forbidden through Eq. (5c).

There exist dark sector interactions that deplete the DM and ensure the correct abundance [1]. Since  $n_{\phi_B} - \bar{n}_{\phi_B}$  is

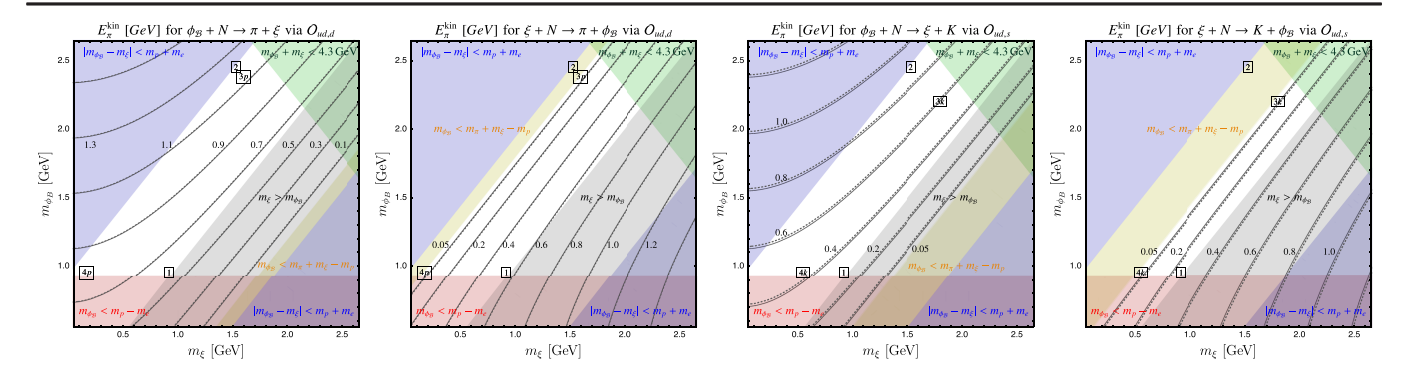


FIG. 2. Parameter space and kinetic energy contours for the eight different DM IND processes arising in mesogenesis. Colored regions are ruled out by kinematics, Eq. (2), or mechanism considerations, Eq. (5). Solid lines correspond to kinetic energy for scattering off protons N = p and the dashed off nucleons N = n. In each panel, we indicate the location of the representative BMs: 1, 2, 3p, 4p for pions and 1, 2, 3k, 4k for kaons as summarized in Table II.

related to the baryon asymmetry,  $\phi_B$  must always constitute some, but not all, of the DM: if  $m_{\phi_B} < m_{\xi}$ , dark interactions could annihilate the entire  $\xi$  population into  $\psi_B$ 's. The measured ratio of DM to baryon densities [37] implies that  $m_{\phi_B} \simeq 5 m_p$ , violating Eq. (5a). This motivates multicomponent DM where we enforce Eq. (5d) so that the symmetric component of  $\phi_B$ 's annihilate into  $\xi$ 's. Since the measured SM baryon asymmetry is always balanced by an asymmetry in  $\phi_B$ 's, the observed DM to baryon ratio  $\rho_{\rm DM} \sim 5 \rho_B$  fixes the expected density of  $\xi$  and  $\phi_B$  particles in the halo:  $\rho_{\xi}/\rho_{\phi_B} = 5 m_p/m_{\phi_B} - 1$ , and  $\rho_{\rm total} = \rho_{\phi} + \rho_{\xi} = 0.4 \ {\rm GeV/cm^3}$ . Given Eq. (5c), there will always be a substantial asymmetric component of DM, and so both INDs in Eq. (2) will be present if kinematically allowed.

The scattering cross sections for the INDs are computed from Eq. (4). We parametrize the cross section as

$$\langle \sigma v \rangle_{\rm DM}^{\mathcal{M}} \equiv \frac{(y_d \times C_{ud_i,d_j})^2}{m_{w_D}^2 ({\rm GeV}^{-4})} \langle \sigma v \rangle_{\rm DM}^{\mathcal{M},0},$$
 (6)

where  $\mathcal{M}=\pi^0$ ,  $\pi^+$ ,  $K^+$ ,  $K^0$ , and  $\mathrm{DM}=\phi_{\mathcal{B}}$ ,  $\xi$ . The range of variation  $m_{\psi_{\mathcal{B}}}\sim 1\text{--}4.3$  GeV is a small effect. Values of the coupling stripped cross section  $\langle \sigma v \rangle_{\mathrm{DM}}^{\mathcal{M},0}$  over the allowed parameter space of Fig. 2 are shown in Table I.

TABLE I. IND allowed by Eqs. (2) and (5), the expected range of unsmeared kinetic energy of the outgoing meson and the stripped cross section defined in Eq. (6).

Initial DM	Final meson	Meson $E_{kin}$ (GeV)	Approx. $\langle \sigma v \rangle_0$ (cm <sup>3</sup> / sec)
$\phi_{\mathcal{B}}$ $\xi$ $\phi_{\mathcal{B}}$	$\pi^+/\pi^0 \ \pi^+/\pi^0 \ K^+/K^0$	0.6–1.2 0.02–0.6 0.3–0.9	$10^{-21.4} - 10^{-21.0}$ $10^{-22.5} - 10^{-21.9}$ $10^{-19.7} - 10^{-19.3}$
ξ	$K^+/K^0$	0.04-0.3	$10^{-20.6} - 10^{-19.8}$

E.g.,  $y_d=0.1$  and  $C_{ud_i,d_j}^{\rm max}$ , the expected cross section can be as large as  $10^{-38}$ – $10^{-36}$  cm<sup>3</sup>/ sec in the allowed parameter space for all channels. Meanwhile, the estimated detector sensitivity is  $\sim 10^{-42}$ – $10^{-40}$  cm<sup>2</sup>/ sec.

Signal Monte Carlo and benchmarks.—We pick benchmark (BM) points to highlight the possible signal topologies; these are defined in Table II and labeled in Fig. 2. For large nuclei, nuclear effects including motion of the nucleons and final state interactions of hadronic particles escaping the nuclear remnant smear the outgoing meson energy, can liberate additional hadrons, and can change the isospin characteristics of the meson. In order to account for these effects, as well as allow for future simulation of the detailed detector response, we have developed a Monte Carlo event generation tool for the IND process.

Signal events are generated using a modified version of GENIE (v3.0.2) [23,24]. We employ the default tune (G18 02a) throughout, though we considered other nuclear models. We found differences in the signal distributions of order 10% between hA and hN models of the intranuclear cascade. The current nucleon decay module in GENIE

TABLE II. BMs highlighting the possible signal topologies. BM 1 corresponds to  $E_{p\phi_{B}\to\mathcal{M}\xi}^{\mathrm{kin,min}}\sim E_{p\phi_{B}\to\mathcal{M}\xi}^{\mathrm{kin,max}}$  for both  $\pi$ 's and kaons. BM 2 corresponds to  $E_{p\phi_{B}\to\mathcal{M}\xi}^{\mathrm{kin,max}}$ . BMs 3p and 3k correspond to the maximal  $E_{p\phi_{B}\to\mathcal{M}\xi}^{\mathrm{kin}}$  such that the incoming  $\xi$  process is still allowed for production of  $\pi$ 's and kaons, respectfully. BMs 4p and 4k highlight a region of  $\{m_{\xi}, m_{\phi_{B}}\}$  that would still lead to a signal for small  $m_{\psi_{B}}$  (see labels in Fig. 2).

Benchmark	$m_{\phi_{\mathcal{B}}}$ (GeV)	$m_{\xi}$ (GeV)
1	0.95	0.92
2	2.45	1.53
3 <i>p</i>	2.38	1.6
3 <i>p</i> 3 <i>k</i>	2.2	1.8
	0.95	0.17
4 p 4 k	0.95	0.55

was modified to allow for IND kinematics. The meson final states currently implemented are  $\pi^0$ ,  $\pi^+$ ,  $K^0_{S/L}$ ,  $K^+$ , and  $D^0$ . This module propagates the outgoing mesons through the nuclear remnant to the edge of the nucleus. The kinematics of the IND process are fixed given masses for the two DM particles. The cross section is determined by Eq. (6). For nonrelativistic DM, there is a small difference in the rate for interaction with a high speed nucleon compared with a nucleon at rest. We neglect this small difference of  $\sim 10\%$ , as well as the nuclear modeling uncertainties, in our sensitivities below.

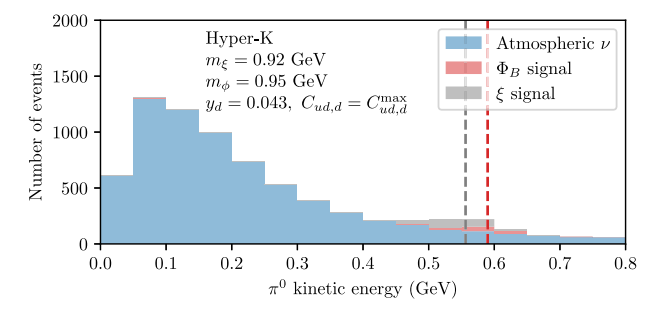
Signals at neutrino experiments.—The current best limits on spontaneous nucleon decays to pions are from Super-Kamiokande [29], which applied a pion momentum cut of 1 GeV and are thus applicable to parts of mesogenesis parameter space—here the experimental limit can be compared to an effective lifetime  $(\tau_N^{\rm IND})^{-1} = n_{\rm DM} \langle \sigma v \rangle_{\rm DM}$ [34,38,39]. This yields an approximate, conservative, limit of  $y_d \times C_{ud,d}/C_{ud,d}^{\text{max}} \gtrsim 0.03-0.1$  for  $70 \lesssim E_{\pi^+}^{\text{kin}} \lesssim 870$  and  $E_{\pi^0}^{\rm kin} \lesssim 870$  MeV. Existing searches in kaon channels [31,32,40] placed narrow ranges of momentum cuts. Consequentially, the majority of parameter space of interest is unconstrained by existing searches. Super-Kamiokande is expected to have sensitivity to IND signals given dedicated studies. Hyper-Kamiokande will improve on this with its larger exposure. Since DUNE is based on liquid argon time-projection chamber technology, it could have particular sensitivity to certain models. Liquid scintillators, e.g., JUNO, have low thresholds and we expect high sensitivity, particularly to charged particles. Our modeling of the different detector responses is described in the Supplemental Material [41].

Sensitivity estimates.—The dominant background is expected to be inelastic scattering of atmospheric neutrinos off nuclei, leading to additional mesons. By looking for off beam timing events, beam-related backgrounds can be evaded. To study the atmospheric neutrino background, we generate atmospheric neutrino events using GENIE (v3.0.2),

along with the Bartol atmospheric neutrino flux model [46] at Soudan for DUNE and Kamioka or all other experiments.

From samples of DM signals and atmospheric neutrino events, we look for events containing the relevant final state meson for the channel considered. Not all events with such a meson should be considered. Signal events contain a single meson and no other activity other than possible emissions from the nuclear remnant or by-products of final state interactions. Thus, it is highly beneficial to veto any activity beyond the expected meson. To do so, we first apply thresholds (described in detail in the Supplemental Material [41]) to all final state particles. Of the remaining particles that can be detected, we veto events that have anything other than a meson of the expected type. For the pion channels, order 1% of atmospheric neutrino scattering events lead to an event matching these criteria. This leaves a search that is not entirely background-free. For the kaon channels, on the other hand, single kaon events are only possible with additional flavor-violating weak interactions. Searches in these channels may thus be background-free if kaon reconstruction is sufficiently good. To get a sense of the events after these vetoes, we plot kinetic energy distributions of the remaining signal and background events; a few illustrative distributions are shown in Figs. 3 and 4.

We now estimate the sensitivity to  $y_d \times C_{ud_i,d_j}/C_{ud_i,d_j}^{\max}$ . For pion channels, we apply the selection described above. To eliminate a majority of the background events, we also require that the selected pion has a kinetic energy within 100 MeV of its unsmeared value Eq. (3). There are significant uncertainties in both the background flux and cross sections. We therefore assume a 30% background normalization uncertainty and determine an estimated  $2\sigma$  sensitivity for the pion channels [47]. For the kaon channels, no further selection is required as we have found that this channel is nearly background-free, and we determine the coupling that would lead to five signal events over the assumed exposure of the experiment.



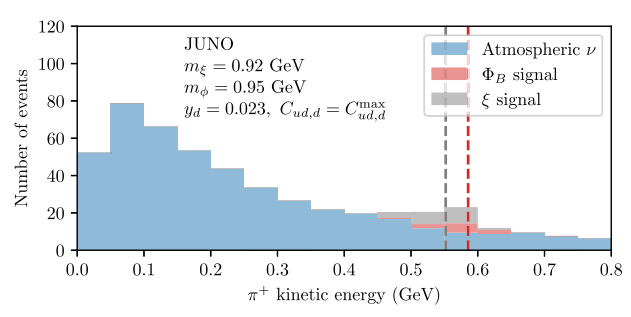


FIG. 3. Kinetic energy distributions for a sample BM model at Hyper-Kamiokande and JUNO. Super-Kamiokande is simply a rescaling of the rate at Hyper-Kamiokande by a factor of 16. Dashed lines indicate the unsmeared energy, Eq. (3). Green lines indicate, where relevant, the assumed threshold for the detector to see the meson. The Hyper-Kamiokande and JUNO signals have a monoenergetic spike corresponding to scattering off hydrogen, while the smeared distribution corresponds to scatterings off oxygen. The couplings are chosen at our estimated threshold of sensitivity.

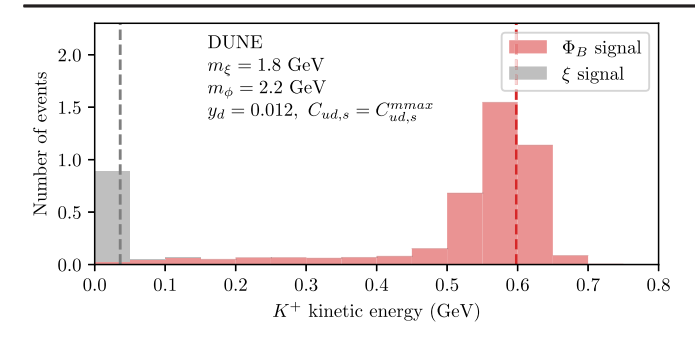


FIG. 4. Kinetic energy distributions for sample BM models at DUNE for the kaon channel with the conventions outlined in Fig. 3.

The sensitivity results are summarized in Table III for the BMs listed in Table II.

Discussion.—This Letter introduced the first direct probe of the DM in mesogenesis: the IND signal. We have chosen BMs, i.e., Table II, that span the entire parameter space in which mesogenesis is possible (as can be seen in Fig. 2). Therefore, an exhaustive search by the experiments discussed here could probe the entire parameter space of DM in mesogenesis down to sensitivities listed in Table. III. Furthermore, our sensitivity estimates in Table III indicate

TABLE III. Estimated coupling sensitivity at DUNE with 400 kton yr of exposure, at Super-Kamiokande with 350.8 kton yr of exposure, at Hyper-Kamiokande with 1900 kton yr of exposure, and at JUNO with 200 kton yr of exposure. We apply the solar minimum flux model for all experiments. The solar maximum model gives slightly different sensitivity estimates. All sensitivities are expressed as the ratio  $y_d(C_{ud_i,d_j}/C_{ud_i,d_j}^{\max})$ ; we have normalized the Wilson coefficients by the maximally allowed value from collider constraints. The fact that all values  $\ll 1$  indicates that IND searches at neutrino experiments are significantly more powerful probes than other existing experiments.

BM	DUNE	Super-K	Hyper-K	JUNO
1 π <sup>+</sup>	0.034	0.10	0.10	0.024
$2 \pi^+$	0.015	0.054	0.054	0.011
$3p \pi^+$	0.087	0.14	0.14	0.046
$4p \pi^+$	0.11	0.18	0.17	0.045
$1 \pi^0$	0.046	0.047	0.046	0.040
$2 \pi^0$	0.023	0.021	0.019	0.020
$3p \pi^0$	0.35	0.32	0.32	0.22
$4p \pi^0$	0.13	0.12	0.12	0.084
1 <i>K</i> <sup>+</sup>	0.012	0.016	0.0070	0.019
$2 K^{+}$	0.0077	0.0097	0.0042	0.011
$3k K^+$	0.012	0.015	0.0065	0.017
$4k K^+$	0.011	0.015	0.0062	0.017
$1 K_S^0$	0.0024	0.0029	0.0012	0.0051
$2 K_{S}^{0}$	0.0049	0.0058	0.0025	0.011
$3k K_S^0$	0.0046	0.0054	0.0023	0.0097
$4k K_S^0$	0.0029	0.0034	0.0015	0.0062

that a null observation would place a more stringent bound on these operators than currently possible with colliders. Figures 3 and 4 show the spectacular signal expected at DUNE, Hyper-Kamiokande, and JUNO for representative benchmark points. Note that DUNE is expected to have slightly better sensitivity to pion channels due to reduced backgrounds. In addition to providing experimentalists with the tools needed to search for DM IND signals at neutrino experiments, this Letter paves the way to a signal-driven model building effort of the dark sector. This work also paves the way to new exploration of additional signal mesogenesis through DM IND in high density astrophysical environments [49], which is the subject of ongoing work.

All data generated using this code are available upon request. The code itself can be downloaded from GitHub [25].

We thank Yun-Tse Tsai for comments on the draft and Yue Zhao for helpful discussions. The work of J. B. is supported by the National Science Foundation under Grant No. 2112789. J. B. thanks the Mainz Institute for Theoretical Physics (MITP) of the Cluster of Excellence PRISMA+ (project ID 39083149) for their hospitality. The research of GE is supported by the National Science Foundation (NSF) Grant No. PHY-2210562, by a grant from University of Texas at Austin.

<sup>\*</sup>Joshua.Berger@colostate.edu †gilly.elor@utexas.austin.edu

<sup>[1]</sup> G. Elor, M. Escudero, and A. E. Nelson, Phys. Rev. D 99, 035031 (2019).

<sup>[2]</sup> G. Elor and R. McGehee, Phys. Rev. D 103, 035005 (2021).

<sup>[3]</sup> F. Elahi, G. Elor, and R. McGehee, Phys. Rev. D 105, 055024 (2022).

<sup>[4]</sup> G. Alonso-Álvarez, G. Elor, A. E. Nelson, and H. Xiao, J. High Energy Phys. 03 (2020) 046.

<sup>[5]</sup> G. Elor and A. W. M. Guerrera, J. High Energy Phys. 02 (2023) 100.

<sup>[6]</sup> G. Alonso-Álvarez, G. Elor, and M. Escudero, Phys. Rev. D 104, 035028 (2021).

<sup>[7]</sup> C. Hadjivasiliou *et al.* (Belle Collaboration), Phys. Rev. D 105, L051101 (2022).

<sup>[8]</sup> A. B. Rodriguez, V. Chobanova, X. Cid Vidal, S. L. Soli no, D. M. Santos, T. Mombacher, C. Prouve, E. X. R. Fernandez, and C. Vazquez Sierra, Eur. Phys. J. C 81, 964 (2021).

<sup>[9]</sup> M. Borsato et al., Rep. Prog. Phys. 85, 024201 (2022).

<sup>[10]</sup> X. Shi (BESIII Collaboration), Proc. Sci. EPS-HEP2021 (2022) 663.

<sup>[11]</sup> G. Elor et al., in 2022 Snowmass Summer Study (2022), arXiv:2203.05010.

<sup>[12]</sup> P. Asadi et al., arXiv:2203.06680.

<sup>[13]</sup> J. L. Barrow et al., arXiv:2203.07059.

<sup>[14]</sup> E. Goudzovski et al., Rep. Prog. Phys. 86, 016201 (2023).

- [15] G. Alonso-Álvarez, G. Elor, M. Escudero, B. Fornal, B. Grinstein, and J. M. Camalich, Phys. Rev. D **105**, 115005 (2022).
- [16] B. Fornal and B. Grinstein, Mod. Phys. Lett. A 35, 2030019 (2020).
- [17] B. Grinstein, C. Kouvaris, and N. G. Nielsen, Phys. Rev. Lett. 123, 091601 (2019).
- [18] A. D. Sakharov, Pis'ma Zh. Eksp. Teor. Fiz. 5, 32 (1967); Usp. Fiz. Nauk 161, 61 (1991).
- [19] M. N. Guinot (DUNE Collaboration), Proc. Sci. NuFact2021 (2022) 231.
- [20] C. W. Walter, *Neutrino Oscillations* (World Scientific, Singapore, 2008).
- [21] M. Yokoyama (Hyper-Kamiokande Proto Collaboration), in Prospects in Neutrino Physics (2017), arXiv:1705.00306.
- [22] Z. Djurcic et al. (JUNO Collaboration), arXiv:1508.07166.
- [23] C. Andreopoulos *et al.*, Nucl. Instrum. Methods Phys. Res., Sect. A **614**, 87 (2010).
- [24] C. Andreopoulos, C. Barry, S. Dytman, H. Gallagher, T. Golan, R. Hatcher, G. Perdue, and J. Yarba, arXiv: 1510.05494.
- [25] J. Berger and G. Elor, "GENIE with Induced Nucleon Decay", v3\_02\_02\_IND, Generator-IND, 10.5281/zenodo .10636737 (2024).
- [26] Which may be identified as a squark in a supersymmetric embedding [4].
- [27] C. McGrew, R. Becker-Szendy, C. B. Bratton, J. L. Breault, D. R. Cady *et al.*, Phys. Rev. D **59**, 052004 (1999).
- [28] D. Wall, W. W. M. Allison, G. J. Alner, D. D. Ayres, W. L. Barrett *et al.* (Soudan 2 Collaboration), Phys. Rev. D **62**, 092003 (2000).
- [29] K. Abe *et al.* (Super-Kamiokande Collaboration), Phys. Rev. Lett. **113**, 121802 (2014).
- [30] K. Abe *et al.* (Super-Kamiokande Collaboration), Phys. Rev. D **95**, 012004 (2017).
- [31] K. Kobayashi et al. (Super-Kamiokande Collaboration), Phys. Rev. D 72, 052007 (2005).
- [32] K. Abe *et al.* (Super-Kamiokande Collaboration), Phys. Rev. D **90**, 072005 (2014).
- [33] Similar considerations were discussed in the context of hylogenesis [34].

- [34] H. Davoudiasl, D. E. Morrissey, K. Sigurdson, and S. Tulin, Phys. Rev. D 84, 096008 (2011).
- [35] Y. Aoki, T. Izubuchi, E. Shintani, and A. Soni, Phys. Rev. D 96, 014506 (2017).
- [36] The corresponding values of  $W_0(W_1)$  for  $\pi^+$  are  $0.038\sqrt{2}$   $(-0.05\sqrt{2})$ , for  $\pi^0$  are 0.038 (-0.05), and, through  $\mathcal{O}_{ud,s}$ , for  $K^+$  are 0.0648 (-0.046) and for  $K^0$  are -0.0648 (0.046).
- [37] N. Aghanim *et al.* (Planck Collaboration), Astron. Astrophys, **641**, A6 (2020); **652**, C4(E) (2021).
- [38] H. Davoudiasl, D. E. Morrissey, K. Sigurdson, and S. Tulin, Phys. Rev. Lett. 105, 211304 (2010).
- [39] J. Huang and Y. Zhao, J. High Energy Phys. 02 (2014) 077.
- [40] A. Abusleme *et al.* (JUNO Collaboration), Chin. Phys. C **47**, 113002 (2023).
- [41] See Supplemental Material at http://link.aps.org/supplemental/10.1103/PhysRevLett.132.081002 for details on detector modeling procedures, which includes Refs. [42–45].
- [42] A. Bueno, Z. Dai, Y. Ge, M. Laffranchi, A. J. Melgarejo, A. Meregaglia, S. Navas, and A. Rubbia, J. High Energy Phys. 04 (2007) 041.
- [43] A. Abusleme *et al.* (JUNO Collaboration), Eur. Phys. J. C 81, 10 (2021).
- [44] J. N. Esquivel,  $\mu/\pi$  separation using convolutional neural networks for the MicroBooNE charged current inclusive cross section measurement, Ph.D. thesis, Syracuse University, 2018.
- [45] K. Abe *et al.* (Super-Kamiokande Collaboration), Phys. Rev. D **94**, 052010 (2016).
- [46] G. D. Barr, T. K. Gaisser, P. Lipari, S. Robbins, and T. Stanev, Phys. Rev. D 70, 023006 (2004).
- [47] See, e.g., [48]—a recent atmospheric neutrino analysis assigns uncertainties of order 20%–25% on cross sections.
- [48] T. Wester *et al.* (Super-Kamiokande Collaboration), arXiv: 2311.05105.
- [49] Note that the effect of DM IND signals on big bang nucleosynthesis (BBN) is expected to be small.  $\rho_n/\rho_p$  will be negligibly affected as the cross section for the IND signal is nearly identical for protons and neutrons. Furthermore,  $n_{\rm DM} \langle \sigma v \rangle_{\rm IND}$  is significantly less than the Hubble rate during the era of BBN when temperatures are on the order of a few MeV. Therefore, we expect the baryon to photon ratio to be negligibly effected.